Structural and Functional Roles of HIV-1 gp41 Pretransmembrane Sequence Segmentation

Asier Sáez-Cirión,* José L. R. Arrondo,* María J. Gómara,* Maier Lorizate,* Ibón Iloro,*
Grigory Melikyan,[†] and José L. Nieva*

*Unidad de Biofísica (CSIC-UPV/EHU) and Departamento de Bioquímica, Universidad del País Vasco, 48080 Bilbao, Spain; and
[†]Department of Molecular Biophysics and Physiology, Rush Medical College, Chicago, Illinois 60612 USA

ABSTRACT   The membrane-proximal segment connecting the helical core with the transmembrane anchor of human immunodeficiency virus type 1 gp41 is accessible to broadly neutralizing antibodies and plays a crucial role in fusion activity. New predictive approaches including computation of interfacial affinity and the corresponding hydrophobic moments suggest that this region is functionally segmented into two consecutive subdomains: one amphipathic at the N-terminal side and one fully interfacial at the C-terminus. The N-terminal subdomain would extend α-helices from the preceding carboxy-terminal heptad repeat and provide, at the same time, a hydrophobic-at-interface surface. Experiments were performed to compare a wild-type representing pretransmembrane peptide with a nonamphipathic defective sequence, which otherwise conserved interfacial hydrophobicity at the carboxy-subdomain. Results confirmed that both penetrated equally well into lipid monolayers and both were able to partition into membrane interfaces. However only the functional sequence: 1), adopted helical structures in solution and in membranes; 2), formed homo-oligomers in solution and membranes; and 3), inhibited gp41-induced cell-cell fusion. These data support two roles for gp41 aromatic-rich pretransmembrane sequence: 1), oligomerization of gp41; and 2), immersion into the viral membrane interface. Accessibility to membrane interfaces and subsequent adoption of the low-energy structure may augment helical bundle formation and perhaps be related to a concomitant loss of immunoreactivity. These results may have implications in the development of HIV-1 fusion inhibitors and vaccines.

INTRODUCTION

HIV-1 relies on the fusogenic activity of the gp120/41 envelope protein to introduce its genetic material into target cells, thereby initiating the infectious cycle (reviewed in Doms and Moore, 2000; Eckert and Kim, 2001). In the currently accepted model, HIV-1 fusion cascade begins with the binding of surface subunit gp120 to target cell receptors. Activation causes the gp41 ectodomain to undergo structural rearrangements toward a final structure that has been crystallographically solved (Chan et al., 1997; Weissenhorn et al., 1997). These include the formation and/or reorientation of a triple-stranded α-helical coiled coil by the amino-terminal heptad repeat domain (HR1). The resulting intermediate filamentous structure is postulated to be simultaneously anchored to viral and target cell membranes, through the transmembrane domain (TMD) and the fusion peptide (FP), respectively. This structure collapses into a folded-in-half six-helix bundle. In this trimeric hairpinlike structure the carboxy-terminal helices (HR2) pack in the

reverse direction against hydrophobic grooves outside the coiled coil, so that the amino- and carboxy-termini are placed at the same end of the molecule. It is thus inferred that the production of the trimeric hairpin might bring membranes into close apposition.

It has been argued that the free energy released by the formation of the helical bundle (estimated to be in the order of 40–60 kT; Melikyan et al., 2000) would suffice to induce membrane fusion (in the order of several tens of kT for the activation energy of hemifusion intermediate formation; see an overview in Lentz et al., 2002). However, it is not straightforward how conformational rearrangements in gp41 would couple mechanistically with the actual membrane merger. In particular, bundle structures determined by x-ray crystallography do not include the pretransmembrane (preTM) sequences linking the HR2 to membrane-embedded anchors (Chan et al., 1997; Weissenhorn et al., 1997). The gp41 preTM linker comprises ~20 amino acids (residues 664–683 of the HIV-1 gp160 precursor). Based on the protease sensitivity of the preTM segment, it has been proposed that this region is a flexible, structurally irregular linker (Weissenhorn et al., 1997). However, if fully extended, preTM sequence might keep the six-helix bundle 70 Å apart from the viral membrane (Fig. 1), i.e., distant from the close contacting dehydrated areas required for membrane fusion initiation.

The gp41 membrane-proximal region is accessible to anti-gp41 broadly neutralizing mAbs such as 2F5, 4E10, and Z13 (Zwick et al., 2001). The antigenic nature of the region is most likely conformationally constrained and varies along the HIV-1 fusion pathway (Sattentau et al., 1995; Gorny and
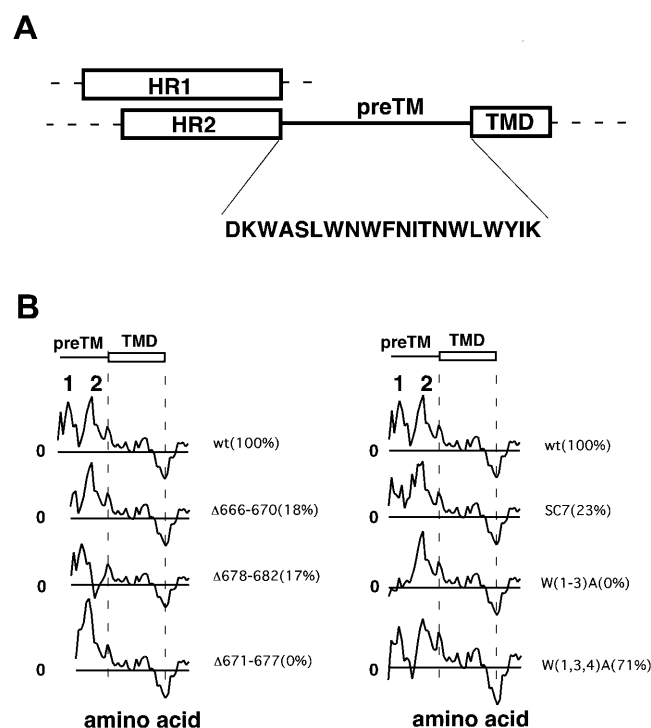
A

B

FIGURE 1 (*A*) Diagram of structural components in HIV-1 gp41 ectodomain and their relative lengths. HR1, HR2, TMD, and the preTM connecting HR2 with TMD have been drawn approximately to scale. Boxes correspond to helical elements and the preTM is displayed as a fully extended chain. Amino acid composition of the preTM sequence comprising residues 664–683 of HIV-1 gp160 precursor is also shown. (*B*) Analysis of interfacial affinity distribution in mutant preTM regions and its correlation with fusogenicity (number of syncytia in the field relative to wild type in *parentheses*) according to Salzwedel et al. (1999) (notation used to designate mutants derived from same reference). Hydropathy-at-interface plots (window = five amino acids) corresponding to residues 661–709 of gp160 precursor (BH10 isolate) were produced as described previously (White and Wimley, 1999; Suárez et al., 2000a) and aligned along invariable TMD sequences. Peaks above the 0 level (*horizontal line*) correspond to positive bilayer-to-water transfer free energy values.

Zolla-Pazner, 2000; Zwick et al., 2001; Parker et al., 2001; Finnegan et al., 2002). Mutational and biophysical analyses have demonstrated that the preTM sequence is instrumental in gp41-mediated fusion (Salzwedel et al., 1999; Muñoz-Barroso et al., 1999; Suárez et al., 2000a,b). This sequence partitions into membrane interfaces, aggregates within, and eventually perturbs the bilayer architecture (Suárez et al., 2000a,b; Saéz-Cirión et al., 2002). NMR spectroscopy detects formation of a well-defined helical structure for monomers in dodecylphosphocholine micelles; therefore an interfacial location with the main axis parallel to the membrane plane has been proposed (Schibli et al., 2001).

Despite these findings, the structural basis of the functional and immunogenic properties of preTM is not understood as yet. We have employed a new approach to the problem by performing the computation of the gp41 preTM hydrophobic-at-interface moment. This parameter indicates that a preTM amphipathic helical segment could segregate

Trp residues and sustain protein-protein and protein-membrane interactions. With the aim of testing this prediction, experiments have been conducted in which we compare the ability of preTM and related sequences to form oligomers and interact with membranes. The results reported in this work sustain the notion that gp41 preTM regions play fundamental structural and functional roles and, as such, represent important targets for the rational development of antiviral therapies.

MATERIALS AND METHODS

Materials

1-Palmitoyl-2-oleoylphosphatidylcholine (POPC) was purchased from Avanti Polar Lipids (Birmingham, AL). Calcein AM and CMAC (CellTracker Blue) were from Molecular Probes (Junction City, OR). *Bis*[sulfosuccinimidyl]suberate (BS^3) was from Pierce (Rockford, IL). D$_2$O, octaethyleneglycol monododecyl ether (C$_{12}$E$_8$), *N*-acetyl-L-tryptophana-mide (NATA), and Triton X-100 were obtained from Sigma (St. Louis, MO). All other reagents were of analytical grade. The sequences, DKWASLWNWFNITNWLWYIK (HIV$_c$) representing the preTM stretch of HIV-1 (BH10 isolate) gp41, its fluorescent derivative (Rho-HIV$_c$) labeled with rhodamine at its N-terminus, and DKAASLANAFNITNWLWYIK (HIV$_{W(1-3)A}$) sequence representing a defective gp41 phenotype (Salzwedel et al., 1999), were synthesized as their C-terminal carboxamides and purified (estimated homogeneity >90%) at the Synthesis Facility of the University Pompeu-Fabra (Barcelona, Spain). Peptide stock solutions were prepared in dimethylsulfoxide (DMSO) (spectroscopy grade).

Hydrophobic moment calculations

To compute the hydrophobic-at-interface moment, we considered the membrane interface-to-water (ΔG_{iwu}) transfer free energies for each amino acid (Wimley and White, 1996) as the moduli of the vectors that project from the main axis of the secondary structure element following the direction of the amino acid side chains (Sáez-Cirión et al., 2003). The hydrophobic moment (μ_H) of a sequence of *N* residues was then calculated as the addition of the *N* hydrophobicity vectors corresponding to the constituent amino acids, following the equation (Eisenberg et al., 1982, 1984):

$$\mu_H = \left(\left(\sum_{n=1}^{N} H_n \sin(\delta n) \right)^2 + \left(\sum_{n=1}^{N} H_n \cos(\delta n) \right)^2 \right)^{1/2}, \quad (1)$$

where H_n is the hydrophobicity of the *n* residue, and δ is the angle formed between side chains of consecutive residues, i.e., 100° for helical conformations.

Preparation of vesicles

Large unilamellar vesicles (LUV) were prepared following the extrusion method of Hope et al. (1985) in 5 mM Hepes, 100 mM NaCl (pH 7.4) buffer. Lipid concentrations of liposome suspensions were determined by phosphate analysis (Böttcher et al., 1961). Mean diameter of vesicles was estimated to be in the range of 100–110 nm by quasielastic light scattering using a Malvern Zeta-Sizer instrument.

Secondary structure determination

Infrared spectroscopy (IR) measurements were conducted essentially as described in Pereira et al. (1997). Samples consisted of floated peptide-lipid complexes obtained in D$_2$O buffer after ultracentrifugation. Solvent samples

were also obtained from the fraction not containing lipid or peptide and subsequently used as background controls. Infrared spectra were recorded in a Nicolet 520 spectrometer equipped with an MCT detector. Samples were placed between two CaF_2 windows separated by 50-μm spacers. A total of 1000 scans (sample) and 1000 scans (reference) were taken for each spectrum, using a shuttle device. Spectra were transferred to a computer where solvent subtraction and band-position determinations were performed as previously reported (Arrondo et al., 1993).

Monolayer penetration

Surface pressure was determined in a fixed-area circular trough (μTrough S system, Kibron, Helsinki). Measurements were carried out at room temperature and under constant stirring. The aqueous phase consisted of 1 ml 5 mM Hepes, 100 mM NaCl (pH 7.4). POPC, dissolved in chloroform, was spread over the surface and the desired initial surface pressure (π_0) was attained by changing the amount of lipid applied to the air-water interface. Peptide was injected into the subphase with a Hamilton microsyringe. At the concentrations used, peptides alone induced negligible increases in surface pressure at the air-water interface.

Partitioning into membranes

Peptide partitioning into membranes was evaluated using POPC LUV (Wimley and White, 1996) by monitoring the change in emitted Trp fluorescence. Corrected spectra were recorded in a Perkin Elmer MPF-66 spectrofluorimeter with excitation set at 280 nm and 5-nm slits. Partitioning curves were subsequently computed from the fractional changes in emitted Trp fluorescence when titrated with increasing lipid concentrations. The signal was further corrected for dilution and inner filter effects as described in White et al. (1998) using the soluble Trp analog, NATA, which does not partition into membranes. The apparent mole fraction partition coefficients, $K_{x(app)}$, were determined fitting the experimental values to an hyperbolic function:

$$F/F_0 = 1 + \frac{[(F_{max}/F_0) - 1][L]}{K + [L]}, \qquad (2)$$

where [L] is the lipid concentration and K is the lipid concentration at which the bound peptide fraction is 0.5. Therefore, $K_{x(app)} = [W]/K$ where [W] is the molar concentration of water.

Peptide oligomerization

Clustering of HIV_c peptide was monitored by the self-quenching effect produced in aggregates of Rho-labeled peptide as described in Ben-Efraim et al. (1999) and Saéz-Cirión et al. (2002). Changes in fluorescence intensity were measured at 581 nm (5-nm slit) with excitation set at 550 nm (5-nm slit). Maximal dequenching (or 0% quenching) was inferred from samples solubilized with Triton X-100 (0.5% v/v). Occasionally, maximal dequenching measurements were carried out in SDS-solubilized samples, always with good correlation. Oligomerization was also evaluated using Tricine-SDS-PAGE. Samples consisted of 45 μg peptide incubated in presence or absence of 20 μM BS[3] bifunctional cross-linking reagent (Knoller et al., 1991). Cross-linked complexes were subjected to gel electrophoresis. Gels were stained with Gelcode blue stain reagent (Pierce, Rockford, IL).

Cell-cell fusion assays

TF228.1.16 cells expressing HIV-1 Env (BH10 strain, a gift from Dr. Z. Jonak, SmithKline Beecham) and HeLaT4^{+} cells expressing CD4 and CXCR4 (obtained from AIDS Research and Reference Reagent Program, NIH) were maintained as described in Melikyan et al. (2000). TF228.1.16 cells (referred to as effector cells) were loaded with fluorescent dye calcein AM (green emission). The target (HeLaT4^{+}) cells were loaded with CMAC (blue emission). Fusion was quantified by fluorescence microscopy by measuring the fraction of cells positive for both dyes out of the total number of effector/target cells in contact, as described in Melikyan et al. (2000). Briefly, effector and target cells were mixed in the presence or in absence of HIV_c or $HIV_{W(1-3)A}$ peptides, allowed to settle on polylysine-coated eight-well chambered slides, and incubated at 37°C for 2 h. Images of calcein and CMAC fluorescence were acquired by intensified charge-coupled device (CCD) camera using appropriate filter sets, digitized, pseudocolored, and overlaid on each other to facilitate detection of cell fusion.

RESULTS

Interfacial hydrophobicity distribution in gp41 preTM sequence

As shown in Fig. 1 A, the gp41 membrane-proximal domain, or pretransmembrane sequence, is located between the carboxy-terminal helix (residues 624–665 of HIV-1 Env precursor) and the transmembrane region (residues 684–706 of HIV-1 Env precursor). In a compelling site-directed mutagenesis analysis of the preTM region, Salzwedel and co-workers (Salzwedel et al., 1999) described the production and functional characterization of 25 gp41 variants. Among these variants, mutants displayed in Fig. 1 B were selected based on the following criteria. We analyzed the deletions and substitutions reported by these authors (full deletion and insertions of epitopes were not analyzed) and established the relationship existing between the capacity of a particular preTM sequence to partition into the membrane interface (Wimley and White, 1996) and the fusogenic activity of gp41 (Salzwedel et al., 1999). When we plot the fusion index versus ΔG for transfer from membranes into water (data not shown), it follows that the wild-type (wt) sequence is the most active, in accord with its largest ΔG value, whose magnitude is linearly related to the fusion index for most substitutions. However, for the group of mutants displayed in Fig. 1 B, the fusion index is much lower. Thus, these sequences showed comparable capability to partition into membranes to that shown by corresponding functional sequences but displayed defective fusion phenotypes. This suggested that, in addition of the overall value, the actual distribution of hydrophobicity (i.e., a structure-related factor) might affect the function of this sequence.

The interfacial hydropathy plots displayed in Fig. 1 B indeed suggest the existence within gp41 preTM of two positive peaks, each comprising ~10 amino acids. Since helical anchors immersed into one monolayer interface might be shorter than TMD anchors (Picot et al., 1994), we calculated average hydrophobicity-at-interface in the plots using small five amino acid windows. Deletions in the preTM region correlated with ablation or merging of the two peaks, and concomitant loss of function. Likewise, the analysis of the triple substitutions and scrambled SC7 mutant suggested that the presence of both peaks might promote fusogenicity. Thus results displayed in Fig. 1 B suggest that gp41 preTM region contains two interfacial segments,

a pattern recently described to occur also in 6K, the alphavirus protein involved in catalyzing membrane fission during viral budding (Sanz et al., 2003). An interfacial sequence containing two hydrophobic-at-interface segments also exists in vesicular stomatitis virus (VSV) glycoprotein membrane-proximal region (data not shown), which is also involved in fusion and budding processes (Robinson and Whitt, 2000; Jeetendra et al., 2002).

The N-terminal gp41 preTM subdomain (*peak 1* in Fig. 1 *B*) would also generate a face with strong affinity for membranes, if folded into an α-helix (Fig. 2). Hydrophobic moments measure the periodicity of residue distribution along the secondary structure elements (Eisenberg et al., 1982, 1984). Preferential orientation of the hydrophobic residues toward one face of the structure element has been proposed to favor hydrophobic interactions between protein structural components and between membranes and protein sequences. Considering that preTM may be part of the soluble gp41 ectodomain (see Discussion), its hydrophobic

moment was computed using the membrane interface-to-water transfer free energies (ΔG_{iwu}) for each amino acid (Wimley and White, 1996; White and Wimley, 1999) as the moduli of the vectors that project following the direction of the amino acid side chains. It must be noted that, when partition from water into interfaces of whole residues is taken into consideration, the relative amino acid hydrophobicities seem to be different from those derived from bulk-phase partitioning of side chains (see for extensive discussions Deber and Goto, 1996; White and Wimley, 1999; Nieva and Suárez, 2000). For instance, nonpolar Val and Ala residues, commonly present in TMD sequences, would not promote partitioning into membranes, whereas aromatic Trp, Tyr, and Phe residues would be efficient promoters. This difference also affects the hydrophobic moment calculation (Fig. 2). According to plots in Fig. 2 *A*, a helical sequence that segregates residues to enable maximal partitioning from water into membranes would be barely detected as amphipathic using Eisenberg hydropathy scale.
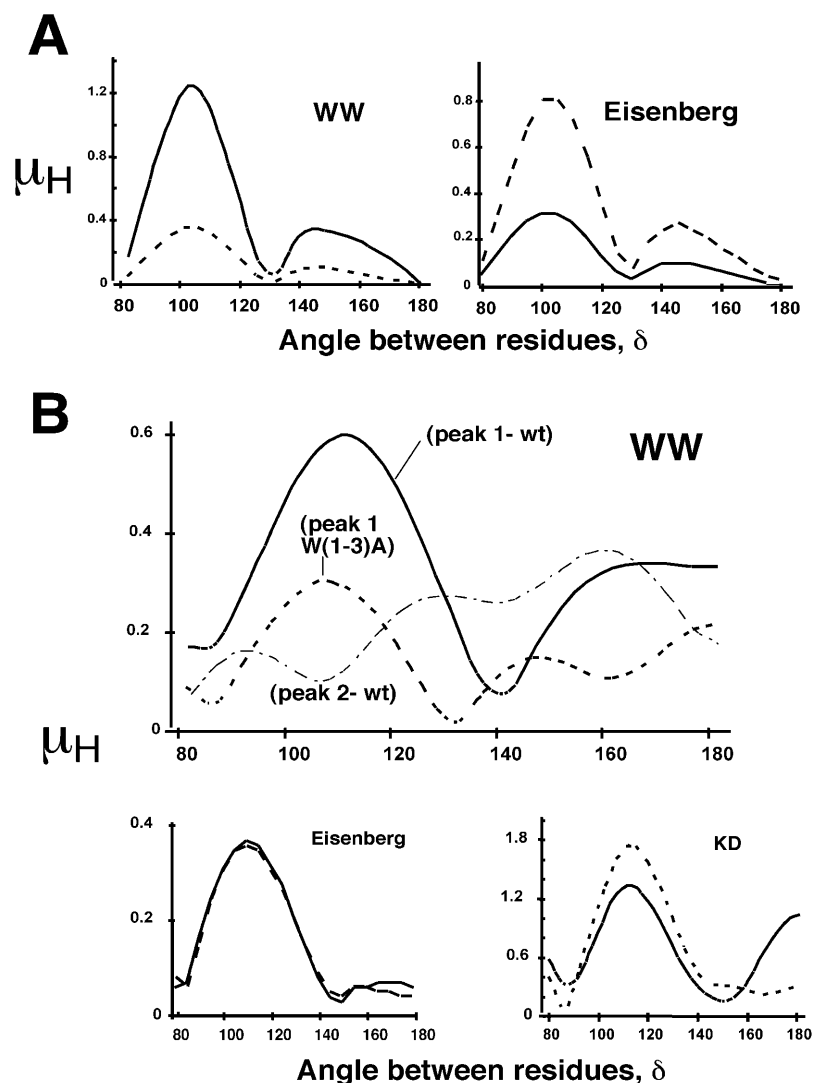

FIGURE 2 Hydrophobic moments (as a function of the δ angle) calculated according to different hydropathy scales. (*A*) Comparison using WW hydrophobicity-at-interface (*left panel*) or Eisenberg hydrophobicity (*right panel*). The selected sequences WWEEWEEWWEEWEE (*solid lines*) and IIRRIRRIIRRIRR (*dotted lines*) contain, alternating with helical periodicity, most hydrophobic and most hydrophilic residues in WW and Eisenberg scales, respectively. (*B*) Hydrophobic moment of the HIV-1 gp160 664–674 segment (~3 helical turns) calculated as a function of the δ angle. Sequences derived from wild-type (*solid lines*) and W(1–3)A mutant (*dotted lines*) proteins are compared using three different hydrophobicity scales (WW, Eisenberg, and KD). Dashed line in WW panel corresponds to the 673–683 gp160 stretch.

Plots in Fig. 2 *B* show the calculated WW moments as a function of the angle between residues (δ). The plot for the amino-terminal preTM segment (*peak 1* in Fig. 1 *B*) displayed a maximum at ~100°, indicating that the adoption of an α-helical conformation generates a Trp-rich surface, whereas the carboxy end (*peak 2* in Fig. 1 *B*) seemed not to be amphipathic. The W(1–3)A triple substitutions within HIV-1 gp41 abrogate its ability to promote cell-cell fusion and virus entry without affecting maturation, transport, or CD4-binding ability of the protein (Salzwedel et al., 1999). These triple Ala substitutions induced the disappearance of the helical interfacial peak of the preTM region. Accordingly, the W(1–3)A mutant also showed a largely reduced moment at $\delta = 100°$ (*top panel* in Fig. 2 *B*). A difference between wt and mutant sequences was not evident when Eisenberg or KD hydropathy scales were applied to calculate the hydrophobic moment (*bottom panels* in Fig. 2 *B*).

In agreement with the previous observations, the sum of moments with fixed $\delta = 100°$ in five-residue windows detected a peak comprising 10 amino acids (residues 663–672 of HIV-1 gp160) at the N-terminus of HIV-1 gp41 preTM (Fig. 3). As shown in Fig. 3, an amphipathic helical motif was present in different HIV-1 isolates and in other lentiviruses. This suggests that the N-terminal segment of gp41 preTM may become an extension of the preceding helical HR2 segment of gp41 ectodomain. This helical HR2 extension shows a tendency to partition into membrane interfaces and is segregated from its C-terminal segment that directly links preTM to the TMD.
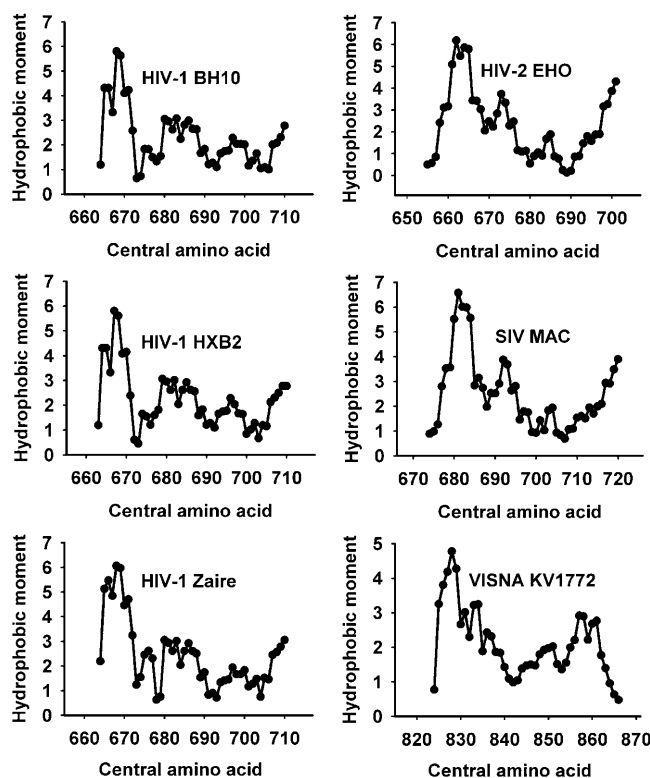

FIGURE 3 Hydrophobic-at-interface moments (sum of the moments in a window of length 11 amino acids) for a fixed $\delta = 100°$ corresponding to preTM-TMD regions derived from different HIV-1 isolates and other lentiviruses. The plotted stretch comprises residues 661–709 of gp160 precursor or homologous sequences in other proteins.

IR analysis of gp41 preTM structure in solution and membranes

The structural changes induced by W(1–3)A substitutions were investigated in solution (Fig. 4 *A*) and membranes (Fig. 4 *B*) by looking at the infrared amide I band located between 1700 and 1600 cm^{-1} (Arrondo and Goñi, 1998, 1999). Deconvolved spectra of HIV$_c$ and HIV$_{W(1–3)A}$ peptides are shown. For HIV$_c$ (*top spectra*) the presence of lipids produces shifts of the 1650 cm^{-1} and the 1629 cm^{-1} components to 1654 cm^{-1} and 1635 cm^{-1}, respectively. On the other hand, in HIV$_{W(1–3)A}$ (*bottom spectra*), the 1626 cm^{-1} band is shifted to 1621 cm^{-1} and two other components at 1644 and 1656 cm^{-1} are present in the presence of lipids. The main component in solution is at 1650 cm^{-1} for HIV$_c$, whereas it is at 1626 cm^{-1} for HIV$_{W(1–3)A}$.

The band at 1650 cm^{-1} ($\approx$60% of total area of HIV$_c$ in solution) can be unambiguously assigned to a canonical α-helix. Assignment of component at 1629 cm^{-1} ($\approx$30% of total area) is not straightforward. Bands below 1635 cm^{-1} together with high frequency components are usually assigned to β-sheet in proteins. However, in oligopeptides short α-helices have been found to display a band around 1635 cm^{-1} (Martinez and Millhauser, 1995); and using ^{13}C-labeled peptides it has been shown that α-helices with a solvated backbone also give rise to signals in that range of wave numbers. Besides, helix-helix interactions in coiled coils also exhibit bands in the region usually attributed to β-sheet (Reisdorf and Krimm, 1996), because of the cross-hydrogen bonds that can be formed. These cross-hydrogen bonds have been described in bacteriorhodopsin (Ubarretxena-Belandia and Engelman, 2001) that also exhibits an anomalous infrared spectrum (Rothschild and Clark, 1979). The presence of lipids produces comparable shifts in both components (to 1654 and 1635 cm^{-1}, respectively) but does not significantly alter the overall structure (55 and 36% of total area, respectively). The former effect can be interpreted either as changes in the geometry of the structural element, or a shift from aqueous to a less polar environment with less strong hydrogen bonds.

To explore further the origin of the 1635 cm^{-1} band, we analyzed IR spectra of HIV$_c$ helices in a membrane milieu. Fluorescence data indicated that rhodamine-labeled HIV$_c$ in lipid vesicles displays a dose-dependent tendency to self-associate (Sáez-Cirión et al., 2002). This is illustrated by results obtained in POPC LUV containing increasing peptide loads (Fig. 5 *A*). Since detergent-solubilized HIV$_c$ is monomeric as judged by SDS-PAGE (see Fig. 7 *A*), Rho-HIV$_c$ fluorescence quenching levels reflect different self-
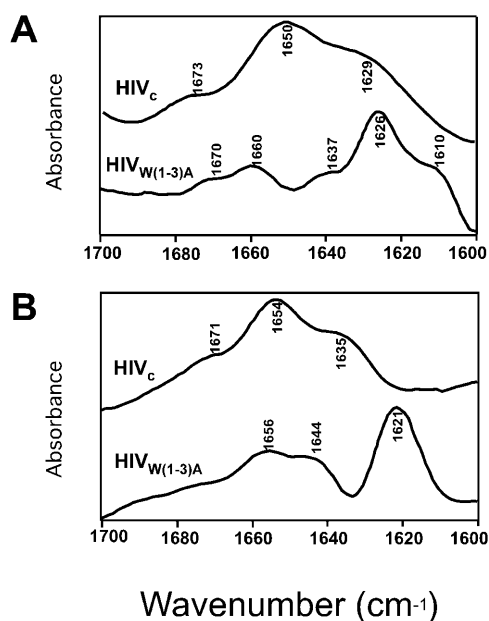
FIGURE 4 Fourier self-deconvolved infrared spectra of HIV_c and $HIV_{W(1-3)A}$ in the amide I region. IR spectra of the peptides were measured in D_2O buffer (*A*) and associated to POPC LUV (*B*). To obtain the latter samples, peptides and vesicles were incubated at 1:250 peptide/lipid mole ratio and lipid-bound peptide was subsequently isolated by flotation in D_2O buffer as previously described (Pereira et al., 1997).

association degrees at the membrane surface. Thus these model membranes provide a tool to assess helical structures as both monomers or multimers. In HIV_c, decreasing the peptide/lipid ratio from 1:50 to 1:1000, where the peptide is most likely monomeric (Fig. 5 *A*), results in a more symmetrical band at 1653 cm^{-1} (Fig. 5 *B*), with no contribution from the component around 1635 cm^{-1}, thus reinforcing the assignment of this band to helix-helix contacts in our system. At the 1:50 ratio where self-association is prominent (Fig. 5 *A*), the α-helical band splits into two components, absorbing at 1656 and 1649 cm^{-1}, besides the presence of a band at 1639 cm^{-1}, as was postulated previously for coiled coils (Reisdorf and Krimm, 1996). The 1:250 peptide/lipid ratio exhibits an intermediate pattern, but is dominated by the band attributed to canonical α-helix at 1653 cm^{-1}.

The structure of $HIV_{W(1-3)A}$ in solution differs from that of HIV_c (Fig. 4 *A*). It has its most intense band at 1626 cm^{-1} ($\approx$47% of total area), indicating an extended conformation of the peptide. Moreover, in the case of this mutant, peptide-lipid binding produces the opposite effect. Rather than keeping a structural organization, the shift downwards to 1621 cm^{-1} of the major component ($\approx$40% of total area), points to a more massive aggregation of the peptide in membranes. The smaller components at 1644 cm^{-1} ($\approx$35%) and 1656 cm^{-1} ($\approx$25%) would indicate the presence of unordered structure and β-turns respectively, as has been shown in all-β proteins such as lectins (Chehin et al., 1999).

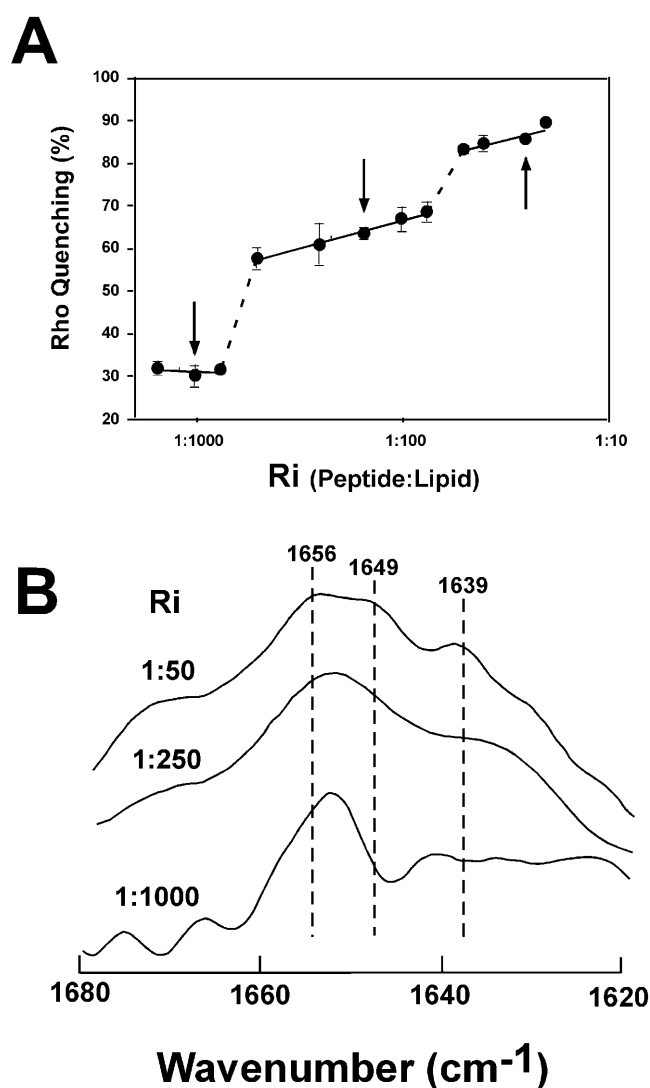In conclusion, the wild-type sequence seems to self-

FIGURE 5 (*A*) Self-association of Rho-HIV_c in POPC membranes. Peptide was incubated with POPC vesicles at the indicated peptide/lipid mole ratios (*Ri*) and the percentage of quenching calculated as previously described (Sáez-Cirión et al., 2002). The quenching levels attained in membranes were independent of the method used to obtain lipid-peptide mixtures, i.e., using either fixed lipid or fixed peptide concentrations. Calculated percentages are mean values $\pm$ SE of four independent determinations. Arrows indicate the *Ri*s selected for IR characterization. (*B*) Fourier self-deconvolved infrared spectra of HIV_c incorporated into POPC membranes. The peptide was added to LUV at the indicated *Ri*s, under the experimental conditions used in the previous panel. Lipid-peptide complexes were subsequently isolated from the floating fractions after ultracentrifugation in D_2O buffer. The spectra are not drawn to the same scale to better show the 1680–1620 amide I region.

associate into helical multimers both in solution and in membranes. In addition, the effect of lipids on both peptides are quite contrasting. Whereas the main conformation of HIV_c is not affected upon its insertion in the lipid bilayer maintaining the solution secondary structure, $HIV_{W(1-3)A}$ stability is disturbed by the presence of lipids, resulting in aggregation-denaturation of the mutant peptide. This con-

firms the predictions in Figs. 2 and 3 and highlights the specific role of Trp residues in stabilizing the sequence folding also in solution.

Gp41 preTM interaction with membranes

The ability of HIV_c and $HIV_{W(1-3)A}$ peptides to penetrate membrane bilayers was first studied by the monolayer technique (Fig. 6 A). The penetration capacity depending on the monolayer surface pressure may be inferred from the monolayer exclusion pressure value (π_{ex}), or initial pressure
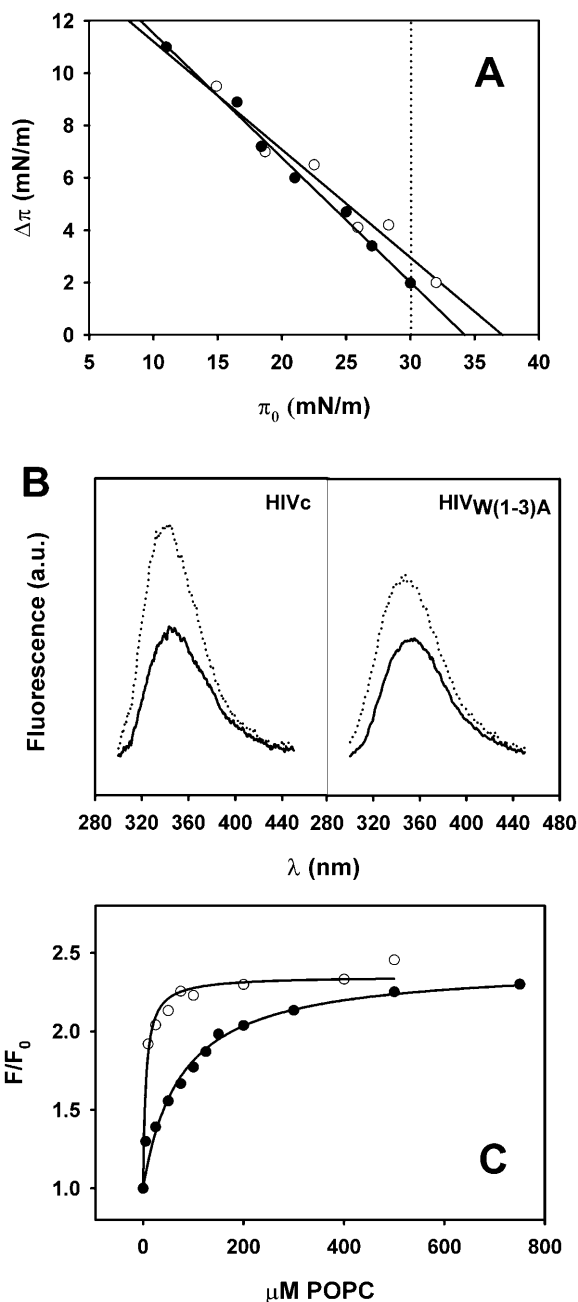
(π_0) at which no increment in pressure is observed after injection of the peptide into the subphase ($\Delta\pi = 0$). The π_{ex} values obtained from plots in Fig. 6 A were 37.2 mN m^{-1} and 34.2 mN m^{-1} for HIV_c and $HIV_{W(1-3)A}$, respectively. Both values are within the range of lateral pressures postulated to arise from the lipid packing density that exists in natural membranes and unstrained bilayers ($\pi_0 \geq 30$ mN m^{-1}; Marsh, 1996).

Consistent with these observations both HIV_c and $HIV_{W(1-3)A}$ were also able to penetrate efficiently lipid bilayers of POPC LUV (Fig. 6, B and C). Results in Fig. 6 B demonstrate that the intrinsic fluorescence of both peptides increased in the presence of these vesicles (*dotted* versus *solid lines*). This is indicative of the Trp residues sensing a low-polarity environment of the lipid bilayer. However, due to the higher Trp content, a higher tendency for HIV_c to spontaneously transfer from water into membranes is expected (Wimley and White, 1996). In accordance with the predictions, titration of the peptides in solution with increasing amounts of lipid vesicles (Fig. 6 C) demonstrated a higher apparent partitioning capacity for the wt-representing peptide, ($K_{x(app)} > 10^7$), compared to the mutant, ($K_{x(app)} \approx 10^6$). The comparable saturation levels observed for both peptides also suggest that membrane-associated species are probably sensing a similar membrane, low-polarity environment. Taken together these data demonstrate that the W(1–3)A mutation did not significantly affect the capacity of the preTM to insert into membranes upon binding (Fig. 6, A and B) but reduced its affinity for the interface (Fig. 6 C).

Gp41 preTM self-association in solution

Experiments were conducted to explore homo-oligomerization of the HIV_c sequence. As shown in Fig. 7 A, HIV_c showed a single band on SDS-PAGE with a molecular weight corresponding to that of a monomer ($\approx$2600 Da). This is consistent with the capacity of the detergent to solubilize Rho-HIV_c peptide oligomers. After subjecting the peptide to chemical cross-linking, oligomers became apparent on the gel. The cross-linking reaction developed similarly when the reagent was present at time = 0, or when added

FIGURE 6 Interaction of HIV_c (*open circles*) and $HIV_{W(1-3)A}$ (*filled circles*) with membranes. (*A*) Penetration of the peptides into POPC monolayers. The maximal increase in surface pressure produced upon injection of peptide in the subphase has been plotted as a function of the initial pressure of the phospholipid monolayer. The dotted line begins at 30 mN/m. (*B*) Fluorescence emission spectra in buffer (*continuous lines*) and incubated with POPC LUV (*dotted lines*). Peptide concentration was 0.5 μM and, in vesicle samples, the peptide/lipid ratio was 1:200. (*C*) Partitioning into membranes. Curves were estimated from the fractional change in Trp fluorescence in the presence of increasing amounts of POPC LUV. The solid lines correspond to the best fits of the experimental values to Eq. 2.
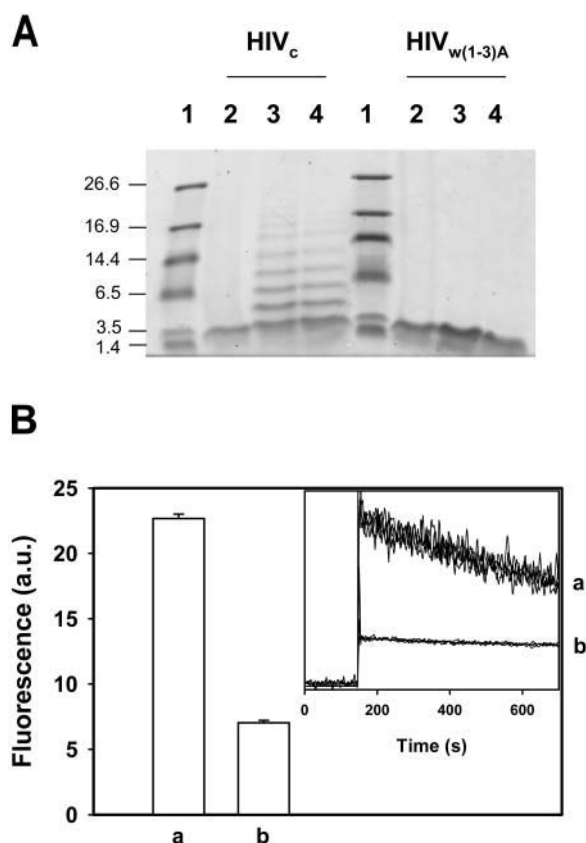
FIGURE 7 Self-association of the gp41 preTM sequence in solution. (A) Oligomerization of HIV$_c$ peptide. HIV$_c$ or HIV$_{W(1–3)A}$ were incubated alone (*lane 2*) or in presence of 20 μM BS^3 for 30 min, added before (*lane 3*), or 90 min after the peptide (*lane 4*). Samples were prepared for SDS-PAGE and resolved on 16.5% Tris-tricine polyacrylamide gels. In the first lane, the molecular weight (kD) markers were run as indicated. (B) Clustering of Rho-HIV$_c$ in solution. Rho emission intensity ($\lambda_{ex} = 550$ and $\lambda_{em} = 581$) was measured 150 s after peptide injection (2-μM final concentration) into buffer. To investigate the effect of replacing Rho-HIV$_c$ with unlabeled HIV$_c$, Rho-HIV$_c$:HIV$_c$ mixtures were incubated at a 1:19 molar ratio. For comparison all intensity values were normalized relative to maximal signal in detergent-solubilized samples. The calculated values of Rho emission values are mean values ± SE of four independent determinations. (*a*) Rho-HIV$_c$:HIV$_c$, 1:19; (*b*) Rho-HIV$_c$. (*Inset*) Time records (four traces per sample) of Rho emission fluorescence in the different samples.

after 90 min of preincubation of the peptide in solution. These oligomers were not observed in the case of HIV$_{W(1–3)A}$ peptide. In summary, the SDS-PAGE analysis suggests the formation of HIV$_c$ homo-oligomers in solution.

This self-association process of HIV$_c$ in solution was subsequently studied using the fluorescently labeled Rho-HIV$_c$ sequence (Fig. 7 *B*). When fluorophore molecules are in close proximity, rhodamine emission diminishes (Hoekstra et al., 1984; Ben-Efraim et al., 1999). Thus, Rho-quenching efficiency correlates with the aggregation state of the peptide (Ben-Efraim et al., 1999; Sáez-Cirión et al., 2002). Experiments in Fig. 7 *B* show that Rho emission decreased with time of incubation in solution (*inset*). When

a fraction of Rho-HIV$_c$ labeled peptide was replaced by unlabeled HIV$_c$ peptide, Rho quenching was hampered (compare *bars a* and *b* in Fig. 7 *B*). This is consistent with the observed fluorescence attenuation due to peptide self-association.

Synthetic preTM peptide specifically inhibits gp41-induced fusion

The ability of preTM to self-associate in solution and membranes raised the possibility of preTM homo-oligomer formation at some stage during gp41-induced fusion process. To explore this hypothesis we tested whether the preTM peptides could interfere with cell-cell fusion induced by HIV-1 envelope (Fig. 8). Co-incubation of the effector and target cells at 37°C in the absence of peptides resulted in extensive fusion, as evidenced by cytoplasmic content mixing between cells. When HIV$_c$ was present in the external solution, it inhibited fusion in a dose-dependent manner showing an apparent IC$_{50}$ value of 577 nM (Fig. 8, *open circles*). In contrast, the mutant HIV$_{W(1–3)A}$ peptide did not suppress fusion even at concentrations as high as 10 μM (*filled circles*). In control experiments, neither of these two peptides inhibited influenza hemagglutinin (HA)-mediated fusion between HA-expressing cells and red blood cells (data not shown). This implies that the inhibitory effect of wt preTM peptide was through its interaction with HIV envelope protein and not through its partitioning into cell membranes and causing nonspecific perturbations. Neither of the two peptides showed a lytic activity on the cells within the concentration range tested here (data not shown).
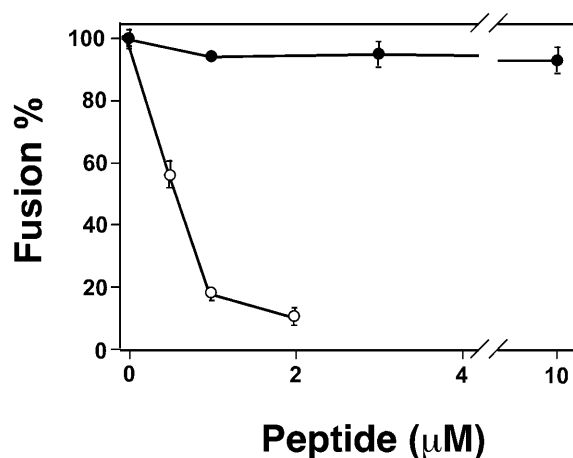

FIGURE 8 Inhibition of HIV Env-induced cell-cell fusion by HIV$_c$ (*open circles*) and HIV$_{W(1–3)A}$ (*filled circles*) peptides. The indicated concentrations of either wt- or mutant-like peptides were added to the mixture of the Env-expressing and CD4$^+$/CXCR4$^+$ HeLaT4$^+$ target cells. Cells were incubated for 2 h at 37°C, and the extent of fusion was determined in at least four independent experiments, as described in Materials and Methods. Bars are SE of mean.

DISCUSSION

PreTM role in membrane anchoring

Truncation of the gp41 carboxy terminus beyond Lys[683] (i.e., last residue of the preTM region) causes loss of membrane anchoring and secretion of the glycoprotein in a soluble form (Dubay et al., 1992; Owens et al., 1994; Salzwedel et al., 1999). This might be interpreted as an indication that the preTM sequence is not sufficient to membrane anchor gp41 with a deleted TMD. However, an inspection of the energetics of helix insertion suggests that a single preTM region might potentially function as a stable interfacial anchor. Estimations of the free energy of inserting the α-helical preTM region (residues 664–683) into membranes as proposed by White and co-workers (White et al., 2001) predicts a low-energy interfacial location, $\Delta G_{\mathrm{ins}} \approx -16$ kcal mol^{-1}, rather than a transmembrane topology, $\Delta G_{\mathrm{ins}} \approx -5$ kcal mol^{-1}. These values may be compared to the energy cost of gp41 TMD (residues 684–706) insertion into membranes: ≈ -9 kcal mol^{-1}, i.e., a value close to that measured for stably inserted glycophorin A TMD (White et al., 2001). Thus, at least in theory, the preTM could anchor the gp41 ectodomain to membranes more stably than does the TMD.

These estimations support the notion that in the mature prefusogenic gp41, the membrane proximal region must be initially folded as a soluble element that becomes membrane bound only after HIV-1 Env activation (Zwick et al., 2001). They also suggest that, in addition to the six-helix bundle, the eventual low-energy state of the protein might comprise a membrane-proximal region immersed into the membrane interface. The fact that preTM region has been shown to bind cholesterol in the context of the full-length envelope protein (Vincent et al., 2002) gives support to this hypothesis. Importantly, recent hydrophobic photolabeling studies have revealed fusion-dependent incorporation of a label into the transmembrane domain and membrane-proximal region of HR2 (Raviv et al., 2003), suggesting the existence after fusion of a membrane-embedded preTM structure connecting both gp41 elements.

PreTM role in oligomerization

One possible means to enhance preTM solubility within the prefusogenic gp41 intermediate is to cluster interfacial residues into an occluded surface. This might be achieved through oligomerization of amphipathic helices. Our hydrophobicity-at-interface distribution analysis suggests that the functional preTM sequence is segmented into two subdomains: one amphipathic at the N-terminal side and one interfacial at the C-terminus (Figs. 1–3). This supports a supplementary role for the preTM sequence in sustaining the prefusogenic gp41 oligomeric organization existing in the virion (Center et al., 2002). However, we caution that membrane partitioning does not seem to be significantly affected by the tendency of preTM peptides to self-associate in solution. We have not observed differences in partitioning at peptide concentrations ranging from 0.1 to 1 μM, and the kinetics of incorporation into membranes of Rho-labeled sequences were similar at 0.1 and 4 μM (i.e., 40 times more concentrated; data not shown). Moreover, the C-terminal segment (residues 674–683 of gp160) contributes enough partitioning energy to enable association with and penetration into membranes, even of denatured sequences (Fig. 6). Thus, partial preTM amphipathicity may potentially contribute to gp41 prefusion structure stability and solubility, but additional factors must exist that preclude membrane exposure of this region before fusion activation.

At any rate, the amphipathic-at-interface N-terminal stretch (residues 664–673) seems to preserve an overall α-helical structure in solution and in membranes (Figs. 4 and 5). IR (Fig. 5) and NMR (Schibli et al., 2001) structural data reveal a monomeric helical structure that would be prevalent in membranes at low doses. This structure self-associates at higher membrane loads or in the presence of raft-type lipids (Sáez-Cirión et al., 2002). Results in this work confirm that preTM may establish helix-helix interactions in solution and in membranes (Figs. 4, 5, and 7).

As depicted in Fig. 9 A, the molecular model for the elongation of HR2 including the preTM amino subdomain shows that hydrophobic HR2 residues implied in packing against the trimeric HR1 coiled coil, and aromatic-interfacial residues might occupy opposite faces of an helix. Thus, a putative oligomeric preTM structure might also help preventing HR2 packing against trimeric HR1 coiled coil. In fact, recent studies demonstrate that HR2 regions are exposed and accessible to inhibitors in native and prefusogenic intermediates of gp41 (Root and Hamer, 2003; Koshiba and Chan, 2003). This mechanism would also be in agreement with the disappearance of mAb 2F5 binding site upon HR1/HR2 complex formation (Gorny and Zolla-Pazner, 2000). The epitope recognized by 2F5 mAb comprises residues 656–671 (Parker et al., 2001), i.e., it includes almost completely the amphipathic preTM amino subdomain. This epitope is recognized at the native prefusogenic form of gp41 and is thought to become occluded upon fusion activation when the six-helix bundle forms (Sattentau et al., 1995; Gorny and Zolla-Pazner, 2000; Finnegan et al., 2002).

Thus, interfacial hydrophobicity could play a role by eliciting the preTM-membrane interaction required to release conformational constraints in HR2 and facilitate HR1-HR2 interactions. Of note, a W(1–5)A mutant in which the 5 Trps have been substituted with Alas induces a defective fusion process arrested at the level of pore opening (see below) (Muñoz-Barroso et al., 1999). This mutant, for which we foresee a defect in preTM-membrane association, is actually more susceptible to inhibition by T20 (Muñoz-Barroso et al., 1999), indicating a defect in bundle formation.
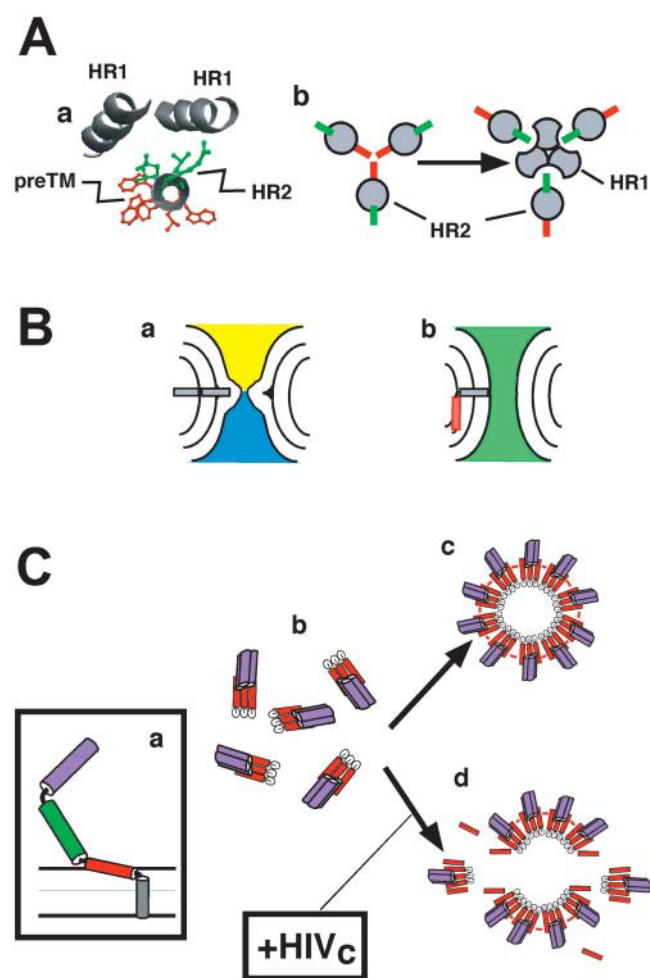
FIGURE 9   Putative roles of interfacial hydrophobicity at gp41 preTM region. (*A*) Assembly of N-terminal amphipathic preTM region would hinder HR1-HR2 interactions. (*a*) Helical model for HIV-1 gp160 652QQEKNEQELLELDKWASLWNWFNIT676 sequence (underlined residues are part of the gp41 HR2 domain). Green side chains denote the residues participating in hydrophobic packing with HR1 helices in the gp41 six-helix bundle crystal structure. Red side chains belong to hydrophobic-at-interface residues of the N-terminal subdomain in the preTM. (*b*) Relative orientation of residues participating in hydrophobic packing with HR1 helices (*green*) and hydrophobic-at-interface residues (*red*) in prefusion (*left*) and postfusion structures (*right*). (*B*) Differential increase of monolayer surface by interfacial preTM may help fusion pore opening. A fractured TMC (*a*) might be brought to opened fusion pore (*b*) after hydrophobic-at-interface preTM (*red*) insertion into *cis*-monolayers. (*C*) Formation of fusion-competent gp41 complexes at the membrane surface. Fusion activation would lead to preTM insertion (*a*). Gp41 trimers (*b*, *top view*) would assemble into fusion-competent arrangements stabilized through preTM interactions (*c*, *top view*). Externally added HIV_c would interfere with the assembly of functional complexes in membranes (*d*, *top view*). PreTM, HR1, and HR2 are designated in red, purple, and green, respectively.

PreTM role in fusion activity and inhibition

Different cell-cell fusion assays demonstrate that gp41 lacking preTM sequence is not fusogenic, i.e., it is incapable of mediating both membrane-and-volume mixing and syncytium formation (Salzwedel et al., 1999; Muñoz-

Barroso et al., 1999). In contrast, several mutants, including aforementioned W(1–5)A, SC7, and Δ678–682, are specifically defective in syncitium formation or complete mixing of cell contents (Muñoz-Barroso et al., 1999). The fusion activity of W(1–5)A mutant, namely, the formation of non-expanding small fusion pores, is similar to that exhibited by GPI-linked hemagglutinin (GPI-HA) of influenza virus (Markosyan et al., 2000). This mutation provokes the elimination of positive hydrophobic-at-interface peaks from preTM region (data not shown). Thus, it appears that in the absence of interfacial hydrophobicity at the preTM region, gp41 displays the activity of ectodomains, which are membrane linked through lipidic tethers. Based on this outcome and our results, we suggest two mutually non-exclusive mechanisms according to which preTM interfacial hydrophobicity could play a role at fusion-pore enlargement (illustrated in Fig. 9, *B* and *C*):

Modulation of monolayer net curvature

Long interfacial preTM sequences seem to be functional in fusion (Salzwedel et al., 1999; Muñoz-Barroso et al., 1999; Suárez et al., 2000a; Jeetendra et al., 2002) and also in membrane fission processes that take part during viral budding (Robinson and Whitt, 2000; Sanz et al., 2003). A low-energy interfacial topology would confer net positive curvature to the preTM-containing membrane monolayer, a factor that might help budding. Conversely, according to the "stalk-pore" hypothesis of fusion, positive curvature in contacting monolayers (*cis*-monolayers) would hinder the formation of a "stalk" (an initial lipidic intermediate that locally connects the *cis*-monolayers of two apposed membranes) (Chernomordik et al., 1995; Siegel and Epand, 1997; Razinkov et al., 1998; Lentz et al., 2000, 2002). Thus, in the framework of this theory, we have to infer that preTM must insert into membranes at later stages of the process. For instance, interfacial preTM structure might promote positive curvature by expanding the *cis*-monolayer in *trans*-monolayer contacts (TMCs), a second lipidic intermediate in the fusion pathway (Fig. 9 *B*). As a result, expansion of fractured single-bilayer diaphragm in the TMC intermediate would be favored (Siegel and Epand, 1997; Lentz et al., 2000). In this way, preTM interfacial hydrophobicity would elicit the eventual opening of fusion pores connecting the initially separated aqueous environments.

Self-assembly of gp41 monomers in membrane surfaces

It has been postulated that an assembly of gp41 oligomers could establish the molecular scaffold that enables membranes to merge. As described by Markosyan et al. (2002), recombinant bundles did not inhibit fusion. Thus, it is unlikely that bundles interact with each other at the fusion site. We propose that the preTM embedded in the viral membrane interface is responsible for self-assembly of gp41

at the fusion site (see also Sáez-Cirión et al., 2002) and, therefore, a defined hydrophobicity distribution along the sequence might condition the rate of formation and/or eventual structure of gp41 complexes. The inhibition data reported in this work (Fig. 8) are consistent with this hypothesis. Our estimations indicate that 99% of the added peptide partitions into membranes under the experimental conditions used in cell-cell fusion experiments. Thus, a likely mechanism of the inhibitory activity of the HIV_c peptide is through its binding to the gp41 cognate preTM region in its membrane-bound state, thereby interfering with functional oligomerization of HIV-1 Env (Fig. 9 C). This inhibition mechanism would be reminiscent of that previously proposed by Kliger et al. (2001) for the T20 peptide.

CONCLUSIONS

Unraveling gp41 preTM structure-function relationship was instrumental in our design of inhibition of cell-cell fusion and may implement anti-HIV drug and vaccine development (Zwick et al., 2001). The hypothesis that stems from our predictions (Figs. 1–3) is that the interfacial hydrophobicity distribution might condition this element's structure function, particularly its tendency to oligomerize as an α-helix in solution and membranes. Experimental data generated so far, including mutagenesis and biophysical characterizations, are consistent with this hypothesis. However, we caution that prefusogenic and postfusogenic gp41 atomic structures, including the membrane-proximal region, are still unavailable. Moreover, even if in the past biophysical characterization of synthetic peptides representing different regions of the HIV-1 gp41 subunit has led to fundamental conclusions on the structural organization and putative mechanism of action of this protein (Doms and Moore, 2000; Eckert and Kim, 2001), we cannot rule out that the structure of these sequences might turn out to be different within full-length gp41.

REFERENCES

Arrondo, J. L. R., and F. M. Goñi. 1998. Infrared studies of protein-induced perturbation of lipids in lipoproteins and membranes. *Chem. Phys. Lipids.* 96:53–68.

Arrondo, J. L. R., and F. M. Goñi. 1999 Structure and dynamics of membrane proteins as studied by infrared spectroscopy. *Prog. Biophys. Mol. Biol.* 72:367–405.

Arrondo, J. L. R., A. Muga, J. Castresana, and F. M. Goñi. 1993. Quantitative studies of the structure of proteins in solution by Fourier-transformed infrared spectroscopy. *Prog. Biophys. Mol. Biol.* 59:23–56.

Ben-Efraim, I., Y. Kliger, C. Hermesh, and Y. Shai. 1999. Membrane-induced step in the activation of Sendai virus fusion protein. *J. Mol. Biol.* 285:609–625.

Böttcher, C. S. F., C. M. van Gent, and C. Fries. 1961. A rapid and sensitive sub-micro phosphorus determination. *Anal. Chim. Acta.* 24:203–204.

Center, R. J., R. D. Leapman, J. Lebowitz, L. O. Arthur, P. L. Earl, and B. Moss. 2002. Oligomeric structure of the human immunodeficiency virus type 1 envelope protein on the virion surface. *J. Virol.* 76:7863–7867.

Chan, D. C., D. Fass, J. M. Berger, and P. S. Kim. 1997. Core structure of gp41 from the HIV-1 envelope glycoprotein. *Cell.* 89:263–273.

Chehin, R., I. Lloro, M. J. Marcos, E. Villar, V. L. Shnyrov, and J. L. R. Arrondo. 1999. Thermal and pH-induced conformational changes of a beta-sheet protein monitored by infrared spectroscopy. *Biochemistry.* 38:1525–1530.

Chernomordik, L., M. M. Kozlov, and J. Zimmerberg. 1995. Lipids in biological membrane fusion. *J. Membr. Biol.* 146:1–14.

Deber, C. M., and N. K. Goto. 1996. Folding proteins into membranes. *Nat. Struct. Biol.* 3:815–818.

Doms, R. W., and J. P. Moore. 2000. HIV-1 membrane fusion: targets of opportunity. *J. Cell Biol.* 151:F9–F13.

Dubay, J. W., S. J. Roberts, B. H. Hahn, and E. Hunter. 1992. Truncation of the human immunodeficiency virus type 1 transmembrane glycoprotein cytoplasmic domain blocks virus infectivity. *J. Virol.* 66:6616–6625.

Eckert, D. M., and P. S. Kim. 2001. Mechanisms of viral fusion and its inhibition. *Annu. Rev. Biochem.* 70:777–810.

Eisenberg, D., R. M. Weiss, and T. C. Terwilliger. 1982. The helical hydrophobic moment: a measure of the amphiphilicity of a helix. *Nature.* 299:371–374.

Eisenberg, D., R. M. Weiss, and T. C. Terwilliger. 1984. The hydrophobic moment detects periodicity in protein hydrophobicity. *Proc. Natl. Acad. Sci. USA.* 81:140–144.

Finnegan, C. M., W. Berg, G. K. Lewis, and A. L. DeVico. 2002. Antigenic properties of the human immunodeficiency virus transmembrane glycoprotein during cell-cell fusion. *J. Virol.* 76:12123–12134.

Gorny, M. K., and S. Zolla-Pazner. 2000. Recognition by human monoclonal antibodies of free and complexed peptides representing the prefusogenic and fusogenic forms of human immunodeficiency virus type-1 gp41. *J. Virol.* 74:6186–6192.

Hoekstra, D., T. De Boer, K. Klappe, and J. Wilschut. 1984. Fluorescence method for measuring the kinetics of fusion between biological membranes. *Biochemistry.* 23:5675–5681.

Hope, M. J., M. B. Bally, G. Webb, and P. R. Cullis. 1985. Production of large unilamellar vesicles by a rapid extrusion procedure. Characterization of size distribution, trapped volume and ability to maintain a membrane potential. *Biochim. Biophys. Acta.* 812:55–65.

Jeetendra, E., C. S. Robison, L. M. Albritton, and M. A. Whitt. 2002. The membrane-proximal domain of vesicular stomatitis virus G protein functions as a membrane fusion potentiator and can induce hemifusion. *J. Virol.* 76:12300–12311.

Kliger, Y., S. A. Gallo, S. G. Peisajovich, I. Muñoz-Barroso, S. Avkin, R. Blumenthal, and Y. Shai. 2001. Mode of action of an antiviral peptide from HIV-1. Inhibition at a post-lipid mixing stage. *J. Biol. Chem.* 276:1391–1397.

Knoller, S., S. Shpungin, and E. Pick. 1991. The membrane-associated component of the amphiphile-activated, cytosol dependent superoxide-forming NADPH oxidase of macrophages is identical to cytochrome b559. *J. Biol. Chem.* 266:2795–2804.

Koshiba, T., and D. C. Chan. 2003. The prefusogenic intermediate of HIV-1 gp41 contains exposed C-peptide regions. *J. Biol. Chem.* 278:7573–7579.

Lentz, B. R., V. Malinin, M. E. Haque, and K. Evans. 2000. Protein machines and lipid assemblies: current views of cell membrane fusion. *Curr. Opin. Struct. Biol.* 10:607–615.

Lentz, B. R., D. P. Siegel, and V. Malinin. 2002. Filling potholes on the path to fusion pores. *Biophys. J.* 82:555–557.

Markosyan, R. M., F. S. Cohen, and G. B. Melikyan. 2000. The lipid-anchored ectodomain of influenza virus hemagglutinin (GPI-HA) is capable of inducing nonenlarging fusion pores. *Mol. Biol. Cell.* 11:1143–1152.

Markosyan, R. M., X. Ma, M. Lu, F. S. Cohen, and G. B. Melikyan. 2002. The mechanism of inhibition of HIV-1 Env-mediated cell-cell fusion by recombinant cores of gp41 ectodomain. *Virology.* 302:174–184.

Marsh, D. 1996. Lateral pressure in membranes. *Biochim. Biophys. Acta.* 1286:183–223.

Martinez, G., and G. Millhauser. 1995. FTIR spectroscopy of alanine-based peptides: assignment of the amide I′ modes for random coil and helix. *J. Struct. Biol.* 114:23–27.

Melikyan, G. B., R. M. Markosyan, H. Hemmati, M. K. Delmedico, D. M. Lambert, and F. S. Cohen. 2000. Evidence that the transition of HIV-1 gp41 into a six-helix bundle, not the bundle configuration, induces membrane fusion. *J. Cell Biol.* 151:413–423.

Muñoz-Barroso, I., K. Salzwedel, E. Hunter, and R. Blumenthal. 1999. Role of the membrane-proximal domain in the initial stages of human immunodeficiency virus type 1 envelope glycoprotein-mediated membrane fusion. *J. Virol.* 73:6089–6092.

Nieva, J. L., and T. Suárez. 2000. Hydrophobic-at-interface regions in viral fusion protein ectodomains. *Biosci. Rep.* 20:519–533.

Owens, R. J., C. Burke, and J. K. Rose. 1994. Mutations in the membrane-spanning domain of the human immunodeficiency virus envelope glycoprotein that affect fusion activity. *J. Virol.* 68:570–574.

Parker, C. E., L. J. Deterding, C. Hager-Braun, J. M. Binley, N. Schulke, H. Katinger, J. P. Moore, and K. B. Tomer. 2001. Fine definition of the epitope on the gp41 glycoprotein of human immunodeficiency virus type 1 for the neutralizing monoclonal antibody 2F5. *J. Virol.* 75:10906–10911.

Pereira, F. B., F. M. Goñi, A. Muga, and J. L. Nieva. 1997. Permeabilization and fusion of uncharged lipid vesicles induced by the HIV-1 fusion peptide adopting an extended conformation: dose and sequence effects. *Biophys. J.* 73:1977–1986.

Picot, D., P. J. Loll, and R. M. Garavito. 1994. The X-ray crystal structure of the membrane protein prostaglandin H2 synthase-1. *Nature.* 367:243–249.

Raviv, Y., M. Viard, and R. Blumenthal. 2003. The dynamics of fusion of HIV and SIV with target cell membranes: a proteomics analysis. *Biophys. J.* 84:L12.

Razinkov, V. I., G. B. Melikyan, R. M. Epand, R. F. Epand, and F. S. Cohen. 1998. Effects of spontaneous bilayer curvature on influenza virus-mediated fusion pores. *J. Gen. Physiol.* 112:409–422.

Reisdorf, W. C., and S. Krimm. 1996. Infrared amide I′ band of the coiled coil. *Biochemistry.* 35:1383–1386.

Robinson, C. S., and M. A. Whitt. 2000. The membrane-proximal stem region of vesicular stomatitis virus G protein confers efficient virus assembly. *J. Virol.* 74:2239–2246.

Root, M. J., and D. H. Hamer. 2003. Targeting therapeutics to an exposed and conserved element of the HIV-1 fusion protein. *Proc. Natl. Acad. Sci. USA.* 100:5016–5021.

Rothschild, K. J., and N. A. Clark. 1979. Anomalous amide I infrared absorption of purple membrane. *Science.* 204:311–312.

Sáez-Cirión, A., M. J. Gómara, A. Agirre, and J. L. Nieva. 2003. Pre-transmembrane sequence of Ebola glycoprotein: interfacial hydropho-bicity distribution and interaction with membranes. *FEBS Lett.* 533:47–53.

Sáez-Cirión, A., S. Nir, M. Lorizate, A. Agirre, A. Cruz, J. Pérez-Gil, and J. L. Nieva. 2002. Sphyngomyelin and cholesterol promote HIV-1 gp41 pretransmembrane sequence surface aggregation and membrane restructuring. *J. Biol. Chem.* 277:21776–21785.

Salzwedel, K., J. West, and E. Hunter. 1999. A conserved tryptophan-rich motif in the membrane-proximal region of the human immunodeficiency virus type 1 gp41 ectodomain is important for env-mediated fusion and virus infectivity. *J. Virol.* 73:2469–2480.

Sanz, M. A., V. Madan, L. Carrasco, and J. L. Nieva. 2003. Interfacial domains in virus 6K protein: detection and functional characterization. *J. Biol. Chem.* 278:2051–2057.

Sattentau, Q. J., S. Zolla-Pazner, and P. Poignard. 1995. Epitope exposure on functional, oligomeric HIV-1 gp41 molecule. *Virology.* 206:713–717.

Schibli, D. J., R. C. Montelaro, and H. J. Vogel. 2001. The membrane-proximal tryptophan-rich region of the HIV glycoprotein, gp41, forms a well-defined helix in dodecylphosphocholine micelles. *Biochemistry.* 40:9570–9578.

Siegel, D. P., and R. M. Epand. 1997. The mechanism of lamellar-to-inverted hexagonal phase transitions in phosphatidylethanolamine: implications for membrane fusion mechanisms. *Biophys. J.* 73:3089–3111.

Suárez, T., W. R. Gallaher, A. Agirre, F. M. Goñi, and J. L. Nieva. 2000a. Membrane interface-interacting sequences within the ectodomain of the HIV-1 envelope glycoprotein: putative role during viral fusion. *J. Virol.* 74:8038–8047.

Suárez, T., S. Nir, F. M. Goñi, A. Sáez-Cirión, and J. L. Nieva. 2000b. The pre-transmembrane region of the human immunodeficiency virus type-1 glycoprotein: a novel fusogenic sequence. *FEBS Lett.* 477:145–149.

Ubarretxena-Belandia, I., and D. M. Engelman. 2001. Helical membrane proteins: diversity of functions in the context of simple architecture. *Curr. Opin. Struct. Biol.* 11:370–376.

Vincent, N., C. Genin, and E. Malvoisin. 2002. Identification of a conserved domain of the HIV-1 transmembrane protein gp41 which interacts with cholesteryl groups. *Biochim. Biophys. Acta.* 1567:157–164.

Weissenhorn, W., A. Dessen, S. C. Harrison, J. J. Skehel, and D. C. Wiley. 1997. Atomic structure of the ectodomain from HIV-1 gp41. *Nature.* 387:426–428.

White, S. H., A. S. Ladokhin, S. Jayasinghe, and K. Hristova. 2001. How membranes shape protein structure. *J. Biol. Chem.* 276:32395–32398.

White, S. H., and W. C. Wimley. 1999. Membrane protein folding and stability: physical principles. *Annu. Rev. Biophys. Biomol. Struct.* 28:319–365.

White, S. H., W. C. Wimley, A. S. Ladokhin, and K. Hristova. 1998. Protein folding in membranes: determining energetics of peptide-bilayer interactions. *Methods Enzymol.* 295:62–87.

Wimley, W., and S. H. White. 1996. Experimentally determined hydrophobicity scale for proteins at membrane interfaces. *Nat. Struct. Biol.* 3:842–848.

Zwick, M. B., A. F. Labrijn, M. Wang, C. Spenlehauer, E. Ollmann, J. M. Binley, J. P. Moore, C. Stiegler, H. Katinger, D. R. Burton, and P. W. H. I. Parren. 2001. Broadly neutralizing antibodies targeted to the membrane-proximal external region of human immunodeficiency virus type 1 glycoprotein gp41. *J. Virol.* 75:10892–10905.